Electronic Supplementary Material (ESI) for Journal of Materials Chemistry C.

Supporting Information Available:

Interlayer Coupling and Optoelectronic Properties of Ultrathin Two-Dimensional Heterostructures based on Graphene, MoS_2 and WS_2

Nengjie Huo,[a] Zhongming Wei,[a] Xiuqing Meng,[b] Joongoo Kang,[c] Fengmin Wu,[b] Shu-Shen Li,[a] Su-Huai Wei*[c] and Jingbo Li*[a,b]

[a]State Key Laboratory for Superlattices and Microstructures, Institute of Semiconductors, Chinese Academy of Sciences, P.O. Box 912, Beijing 100083, China. E-mail: jbli@semi.ac.cn

[b]Research Center for Light Emitting Diodes (LED), Zhejiang Normal University, Jinhua 321004, China

[c]National Renewable Energy Laboratory, Golden, Colorado 80401, USA. E-mail: suhuai.wei@nrel.gov

Optical properties of individual MoS_2, WS_2 and graphene

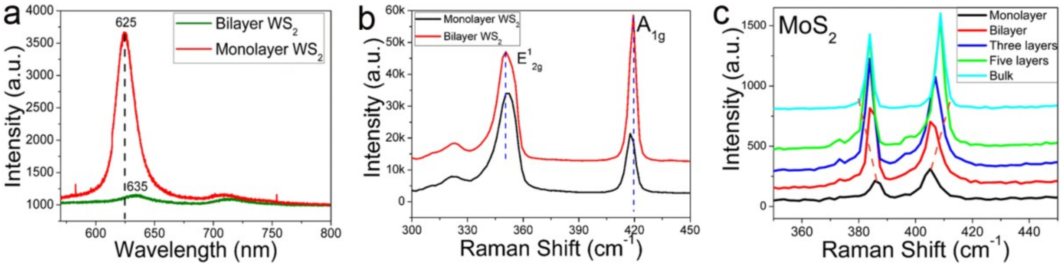

Fig. S1 (a) Photoluminescence (PL) and (b) Raman spectra of monolayer and bilayer WS_2. (c) Raman spectra of MoS_2 with increasing number of layers (from monolayer to bulk).

The PL spectra of WS_2 layers are shown in Fig. S1a, where the significantly increased PL intensity and blue-shift of PL peak from bilayer to monolayer indicate the indirect-to-direct bandgap transition. Furthermore, the phonon frequency of atomically thin MS_2 (M = W or Mo) layers also exhibit unique thickness dependence, that is the Raman active mode A_{1g} (out-of-plane displacement of S atoms) stiffens and the E^1_{2g} (in-plane displacement of M and S atoms) softens with increasing number of layers as seen in Fig. S1b for WS_2 and Fig. S1c for MoS_2 which is consistent with previous reports[S1,S2].

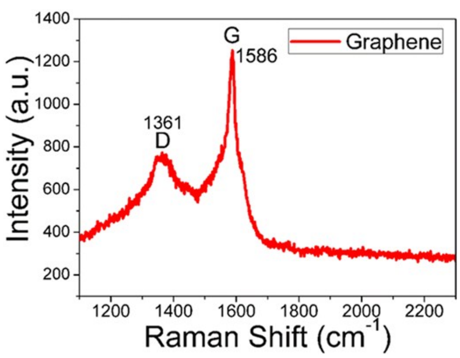

Fig. S2 Raman spectra of graphene, showing the typical Raman modes of graphene: G peak at 1586 cm^{-1} and D peak at 1361 cm^{-1}.

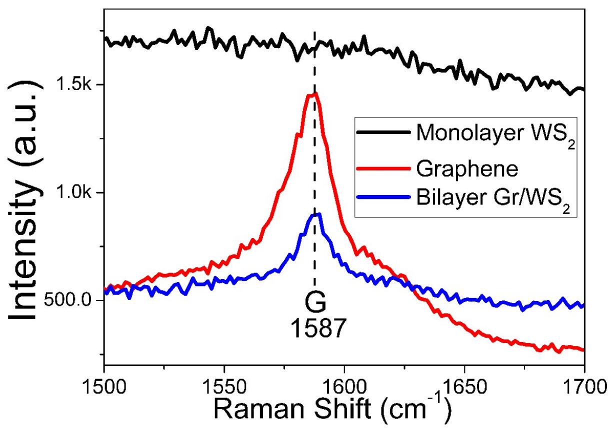

Fig. S3 Raman spectra of monolayer WS_2, graphene, and bilayer Gr/WS_2 from 1500 to 1700 cm^{-1}. Though the the Raman modes A_{1g} and E^1_{2g} of WS_2 in this heterostructure much stiffen compared to that in isolated WS_2 monolayer due to strong interlayer coupling between graphene and WS_2, the G peak of graphene is unchanged suggesting the strong in-plane sp^2 bond in graphene is not much affected by the interlayer interaction.

Electrical and photoresponse properties of individual MoS_2, WS_2

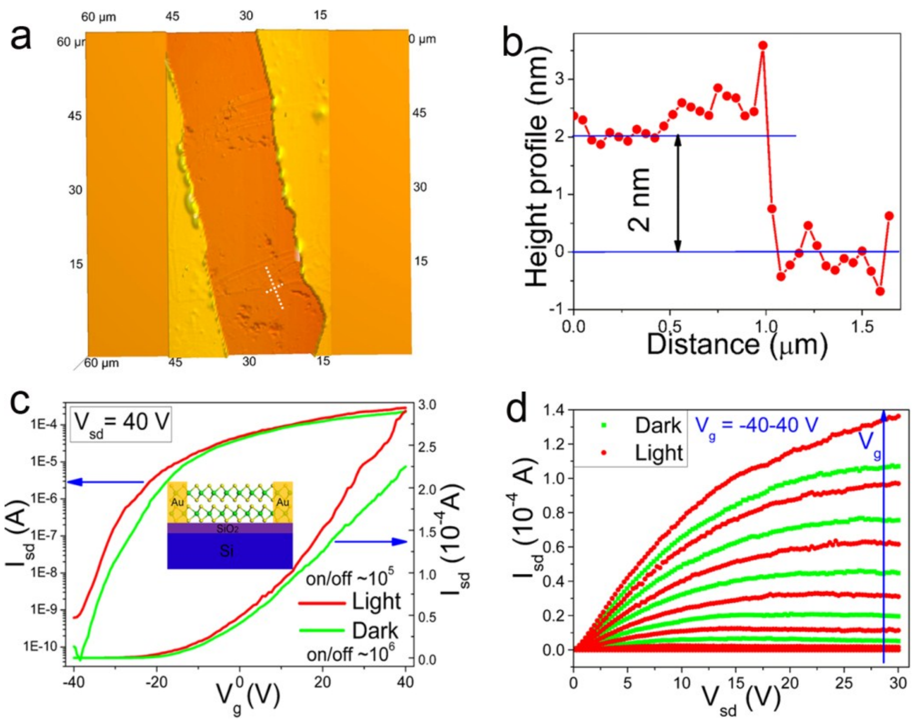

Fig. S4 AFM images of atomically thin MoS_2 transistors (a) with thickness of 2 nm from the cross-sectional plot (b), corresponding to 3-4 layers of MoS_2. (c) Transfer and (d) output characteristic of ultrathin MoS_2 under dark and light illumination (173 μW/cm^2), the inset of (c) corresponds to the schematic diagram of transistor based on few-layer MoS_2.

Transistors made of ultrathin MoS_2 and WS_2 layers are fabricated. The thickness of MoS_2 is 2 nm from atomic force microscope (AFM) images (Fig. S4a and S4b) corresponding to 3-4 layers of MoS_2, and the schematic diagram of few-layer MoS_2 based transistor is shown in the inset of Fig. S4c. From the measured transfer and output characteristics shown in Fig. S4c and S4d, the few-layer MoS_2 transistor exhibits n-type behavior with the on/off ratio as high as 5×10^6. The electron mobility (μ) can be obtained from the equation $\mu = \frac{\partial I_{sd}}{\partial V_g}(\frac{L}{WC_iV_{sd}})$, where L is the channel length, W is the channel width, and C_i is the gate capacitance between the channel and the silicon back gate per unit area, which can be given by equation $C_i = \varepsilon_o \varepsilon_r / d$, ε_o (8.85×10^{-12} F/m) is vacuum dielectric constant, and ε_r (3.9) and d (300 nm) are dielectric constant and thickness of SiO_2, respectively. The calculated electron mobility is 10.3 cm^2/Vs, which is comparable and even higher than previous studied few- or monolayer MoS_2[S3-S5]. Under visible light illumination, the source-drain current I_{sd} is significantly increased at the same gate voltage V_g (Fig. S4c) or source-drain voltage V_{sd} (Fig. S4d), indicating the few-layer MoS_2 is sensitive to visible light. We also notice that the photocurrent is more obvious and the photosensitive on/off ratio (defined as I_{light}/I_{dark}) is larger under negative V_g compared to that under positive V_g. At Off-state (negative V_g), the carriers in MoS_2 layers are consumed so the photo-generated electron and hole carriers are dominating, leading to high photosensitivity (high on/off ratio). Whereas, at On-state (positive V_g), the photo-generated carriers are not prominent because of the existence of high concentration of gate-induced carriers. As a result, the field-effect on/off ratio under light (5×10^5) is decreased by one order of magnitude compared to that under dark.

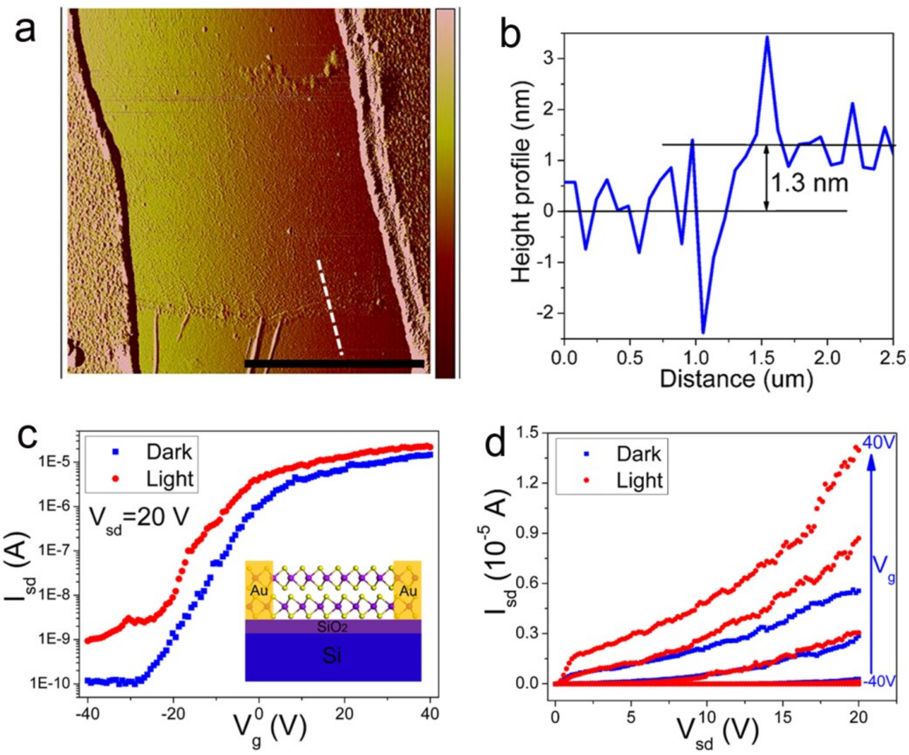

Fig. S5 AFM images of atomically thin WS_2 transistors (a) with thickness of 1.3 nm from the cross-sectional plot (b), corresponding to 2 layers of WS_2. The scale bar in (a) is 5 μm. (c) Transfer and (d) output characteristic of ultrathin WS_2 under dark and light illumination (173 μW/cm^2), the inset of (c) is the schematic diagram of few-layer WS_2 transistor.

The thickness of WS_2 is 1.3 nm corresponding to 2 layers of WS_2 form AFM images (Fig. S5a and S5b), and the inset of Fig. S5c shows the schematic diagram of the device. The transfer and output characteristics of few-layer WS_2 transistors are shown in Fig. S5c and S5d, respectively. The bilayer WS_2 also exhibits an n-type behavior with the on/off ratio as high as 10^5 under dark. The calculated electron mobility is 1.86 cm^2/Vs. Similar to MoS_2, WS_2 can also sensitively respond to the visible light and the photocurrent also become more obvious at Off-state, indicating the gate modulation of photocurrent.

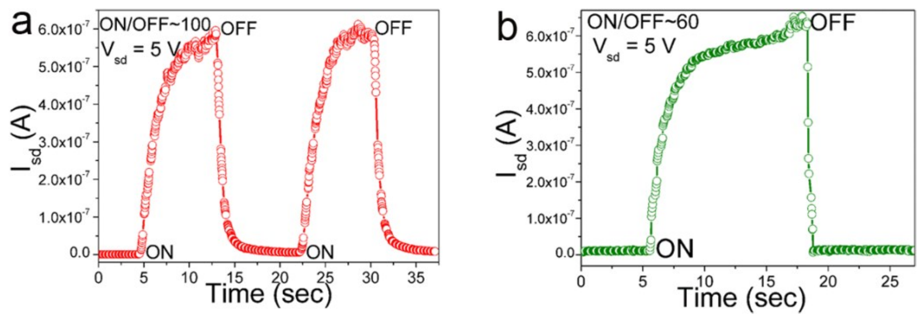

Fig. S6 Time dependences of source drain current I_{sd} of (a) MoS_2 and (b) WS_2 transistors during the visible light (1.36 mW/cm^2) switching on/off at V_{sd} = 5 V without gate voltage.

The dynamic response of the transistors based on ultrathin MoS_2 and WS_2 are also investigated during the light switching on/off as shown in Fig. S6a and S6b, respectively. Under light illumination, photocurrent can be generated resulting in the "On" state of the devices, and the devices can work between "On" and "Off" states fast and reversibly during light turned on/off with photosensitive on/off ratio of about 100 times for MoS_2 and 60 times for WS_2. The response time is about 7 s and 5s for MoS_2 and WS_2, respectively.

P-type behavior of graphene

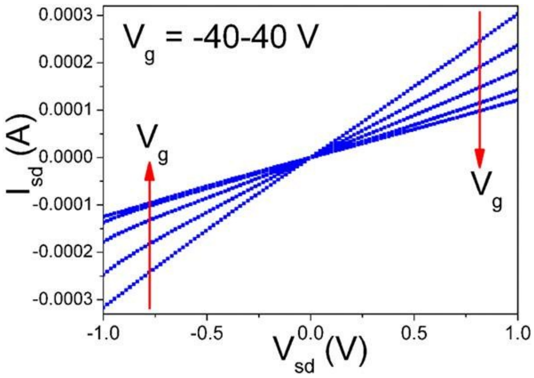

Fig. S7 Output characteristics of graphene, indicating the p-type behavior of graphene.

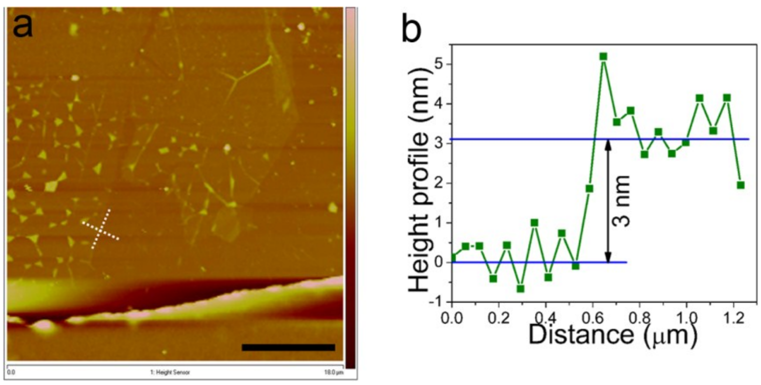

Fig. S8 AFM images of Gr/WS_2 heterostructure (a), and the cross-sectional plot (b) determines the thickness of the heterostructures to be 3 nm. The scale bar in (a) is 5 μm.

Bipolar behavior of Gr/WS_2 heterostructure

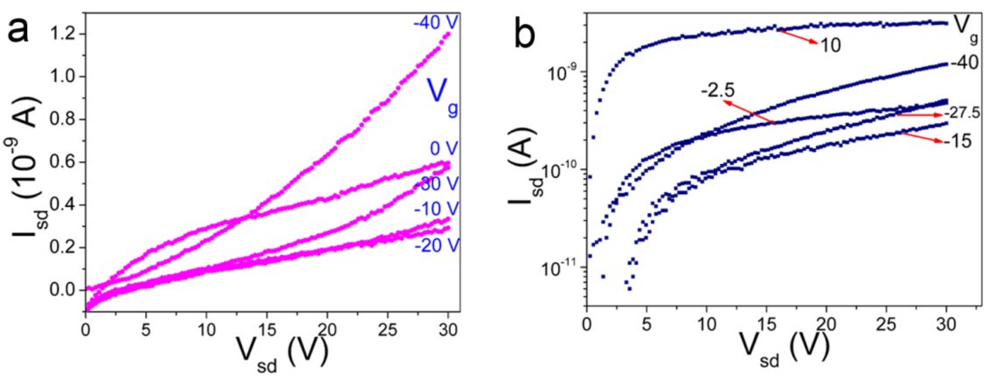

Fig. S9 Output characteristics of Gr/WS_2 heterostructure on linear scale (a) and log scale (b), exhibiting the typical bipolar behavior.

Novel field-effect and photoresponsive properties of MoS_2/WS_2 heterostructures

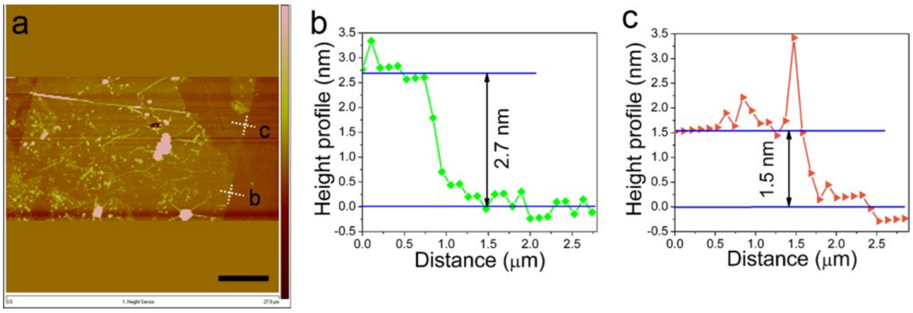

Fig. S10 AFM images of MoS_2/WS_2 heterostructure (a). The total thickness of the heterostructure is 2.7 nm (b), and the thickness of bottom WS_2 layers is 1.5 nm (c), corresponding to 2-3 layers of WS_2 and 2 layers of MoS_2 in the heterostructure. The scale bar in (a) is 5 μm.

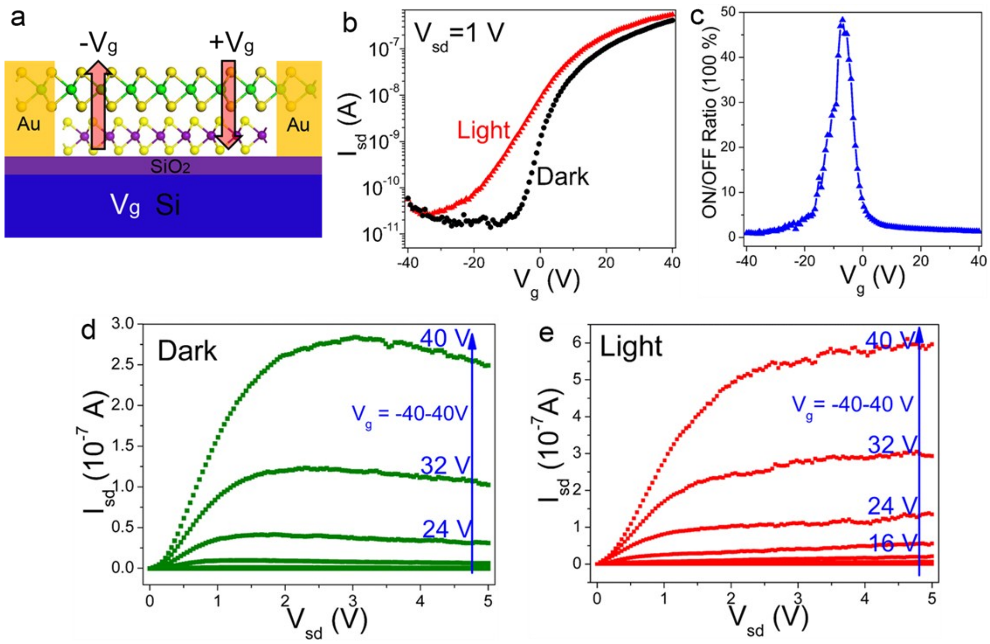

Fig. S11 (a) Schematic diagram of the transistors based on MoS_2/WS_2 heterostructure with both Au electrodes located on top of MoS_2. (b) Transfer characteristics of the device under dark and light illumination (173 μW/cm^2). (c) Photocurrent on/off ratio of the device defined as I_{photo}/I_{dark} under different gate voltage, indicating the gate-tunable photocurrent. Output characteristics of

MoS_2/WS_2 heterostructures under dark (d) and light illumination (e), showing the carrier leakage from top MoS_2 into bottom WS_2 under dark induced by the positive V_g and the photocurrent from WS_2 to MoS_2 can complement this V_g-induced electrons leakage.

There are lots of heterostructure-induced effects in the MoS_2/WS_2 heterostructure based transistors. In the fabrication process, WS_2 with a thickness of about 1.5 nm (~2-3 layers) is covered by 1.2 nm MoS_2 (~2 layers), and the source-drain electrodes are located on top of heterostructure as shown in the AFM images (Fig. S10). A schematic diagram of the device can be seen in Fig. S11a. The total electron density in the heterostructure is determined by the applied V_g, but the current density would dominantly come from the electrons in the top MoS_2 layer. The charge transfer between the two layers can be tuned by V_g, and this induces an interesting electrical transport property. By applying the positive V_g, the gate-induced electrons in MoS_2 will transfer into the bottom WS_2 acting as trap and leading to the reduced On-state current. Hence the on/off ratio of heterostructures ($>10^4$) is decreased compared with that in individual MoS_2 layers (as shown in the transfer curves, Fig. S11b). However, the threshold voltage (V_T) of the heterostructures is increased to -7 V, indicating that the heterostructures facilitate the carrier depletion with the presence of WS_2 trap. From the output characteristics (Fig. S11d), the source drain current I_{sd} under dark reaches maximum at first, and then drops down under positive V_g with increasing V_{sd}. Because the positive V_g induces electrons transfer from MoS_2 to WS_2. It is interesting to note that the I_{sd} can reach saturation under light illumination (Fig. S11e). This is benefit from the generation of photocurrent from WS_2 to MoS_2 which complements the V_g-induced electrons leakage. On the contrary, the negative V_g induces the electrons transfer from WS_2 into MoS_2, resulting in the “quasi-bipolar” transport behavior. Under high negative V_g, some electrons in WS_2 layers are repelled into the MoS_2 layers, leading to the slightly increased I_{sd} with increasing negative V_g. Thus the “p-type” behavior is obtained (Actually, the conducting carriers are still electrons).

Furthermore, the photocurrent can also be modulated by V_g. The photocurrent is non-significant under high (negative or positive) V_g, and the photosensitive on/off ratio can reach the maximum at V_T (Fig. S11c). When $V_g > V_T$, large amounts of carriers are induced by increased V_g leading to high dark current and large total electrons density, together with the unobvious photo-excited carriers and low photosensitive on/off ratio. When $V_g < V_T$, the device is turned off, so dark current is low and slightly increased due to the electrons transfer from bottom WS_2 as discussed above. But the photocurrent under light illumination still drops down with decreased V_g. Thus, the photosensitive on/off ratio is also decreased with increased negative V_g.

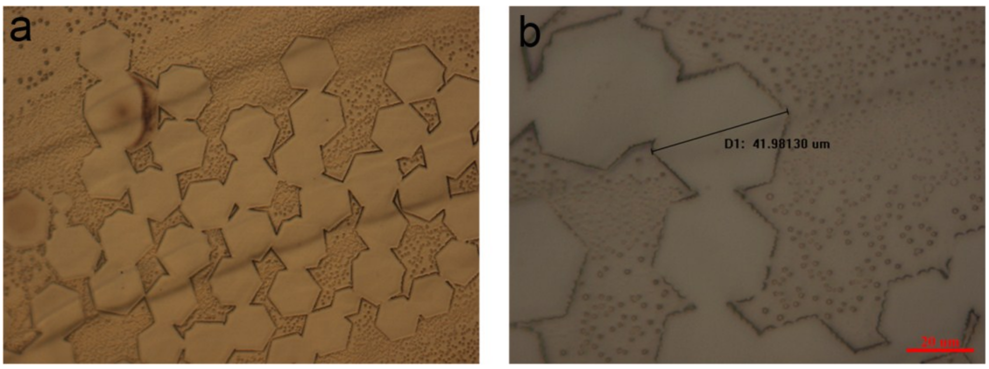

Fig. S12 Optical microscope images of hexagonal single-crystalline graphene with large-size of about 40 μm synthesized by liquid copper CVD method.

References

S1. Lee, C. *et al*. Anomalous Lattice Vibrations of Single- and Few-Layer MoS_2. *ACS Nano* **4**, 2695-2700 (2010).

S2. Zhao, W. *et al*. Lattice dynamics in mono- and few-layer sheets of WS_2 and WSe_2. *Nanoscale* **5**, 9677-9683 (2013).

S3. Lee, Y. H. *et al*. Synthesis and Transfer of Single-Layer Transition Metal Disulfides on Diverse Surfaces. *Nano Lett*. **13,** 1852-1857 (2013).

S4. Novoselov, K. S. *et al*. Two-dimensional atomic crystals. *Proc. Natl Acad. Sci. USA* **102,** 10451-10453 (2005).

S5. Radisavljevic, B., Radenovic, A., Brivio, J., Giacometti, V. & Kis, A. Single-layer MoS_2 transistors. *Nat. Nanotechnol.* **6,** 147-150 (2011).